3

Carbon versus Other Light Elements in Earth's Core

JIE LI, BIN CHEN, MAINAK MOOKHERJEE, AND GUILLAUME MORARD

3.1 Introduction

Carbon is a candidate light element in Earth's core.[1–3] The core consists of a liquid outer shell ranging from 2971 to 5210 km in depth and a solid inner sphere with a radius of 1220 km.[4] Without direct samples, its iron-dominant composition has been inferred from seismological, geochemical, and cosmochemical observations, together with mineral physics constraints from laboratory measurements and theoretical simulations. Both the outer and inner cores are lighter than iron or iron–nickel alloys at relevant pressure–temperature (*P*–*T*) values, indicating the presence of one or more elements with smaller atomic numbers than iron.[5] Candidates for the light alloying elements of the core include hydrogen (H), carbon (C), oxygen (O), silicon (Si), and sulfur (S).

Earth's core may be the largest repository for terrestrial carbon. As the fourth most abundant element in the solar photosphere, carbon occurs in carbonaceous chondrites and ordinary chondrites as a major or minor element.[6] The silicate Earth is depleted in carbon with respect to CI chondrite by more than two orders of magnitude, and by five- to ten-fold after accounting for evaporative loss to outer space during accretion.[7] Some of the missing carbon in the silicate Earth is likely found in its core, considering the large solubility of carbon in the iron-rich melt[8–10] and the strong affinity of carbon for iron metal during core–mantle differentiation.[11–14] Core sequestration can also explain the ^{13}C enrichment in silicate Earth relative to Mars, Vesta, and chondrites.[15] Cosmochemical and geochemical considerations suggest that the core may contain as much as 1 wt.% (5 at.%) carbon.[15] A lower estimate of 0.2 wt.% carbon in the core is derived by assuming that carbon depletion follows the volatility trend.[7] More details are found in Chapter 2. A core containing 1 wt.% carbon would exceed the combined budget of known carbon in the atmosphere, hydrosphere, biosphere, crust, and mantle by one order of magnitude (Figure 3.1). Even with the lowest estimate of 0.1 wt.% carbon, the core would still account for more than half of Earth's total carbon budget.

Constraining the carbon budget of the core is crucial for identifying Earth's building blocks and reconstructing its accretion history. In this chapter, we review constraints on the carbon content of the core from the phase relation, density, and sound velocities of iron–carbon alloys and compare carbon with other light elements in terms of their ability to

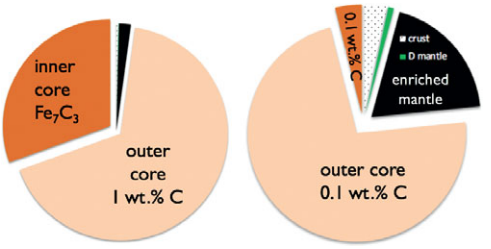

Figure 3.1 Pie diagrams showing the relative sizes of Earth's carbon reservoirs for two end-member models. The concentrations of carbon are assumed to be 0.2 wt.%, 20 ppm, and 165 ppm in the crust, depleted mantle, and enriched mantle, respectively.[16] With 100 ppm in the atmosphere, biosphere, and hydrosphere,[16] the total carbon in these reservoirs is negligible and hence not shown.

match the physical properties of the core. We will also provide a brief discussion of how carbon may have redistributed among various Earth reservoirs through geological time.

3.2 Constraints on Carbon versus Other Light Elements in Earth's Core

3.2.1 Constraints from Phase Relations of Iron–Light Element Systems

Carbon as a core component has attracted special attention through the proposal of a carbide inner core.[9] Based on long extrapolations of equation of state (EoS) data available at the time, Fe_3C with 6.67 wt.% C was predicted to be the first phase to crystallize from an Fe–S–C liquid to form the inner core, even for carbon contents below 1 wt.%.

Testing the model of a carbide inner core requires knowledge of the phase relations at core pressures. As an initial step, the simplified Fe–C binary system has been investigated through experiments and thermodynamic modeling (Figure 3.2). At 1 bar, the system has a eutectic point between iron and Fe_3C at 4.1 wt.% carbon.[17] At pressures above 10 GPa, the eutectic point lies between iron and Fe_7C_3 with 8.41 wt.% carbon,[18] hence Fe_7C_3 is expected to solidify from any composition on the carbon-rich side of the eutectic point at core pressures.

While some studies support the predicted shift of the eutectic composition toward the iron end member with increasing pressure,[19,20] others conclude that the eutectic composition contains 3 ± 1 wt.% carbon between 40 and ~100 GPa in pressure[21] and ~2 wt.% carbon at the pressure of the inner core boundary (ICB).[22] If the outer core contains less carbon than the eutectic composition, then a hexagonal close-packed (hcp) Fe incorporating carbon instead of Fe_7C_3 would be the liquidus phase to form the inner core.

The carbide inner core model can also be tested against the density increase across the ICB. Isochemical freezing of pure Fe or an Fe–light element (Fe–L) alloys produces 1.7% or 2.4% increases in density.[23,24] These are smaller than the 0.6–0.9 g/cm^3 or 4.7–7.1% observed density increases,[25] suggesting that the inner core contains less of the light elements than the outer core. In the ICB condition, a candidate Fe–L composition must reproduce the observed density contrast. For a simplified Fe–L binary, a match is possible

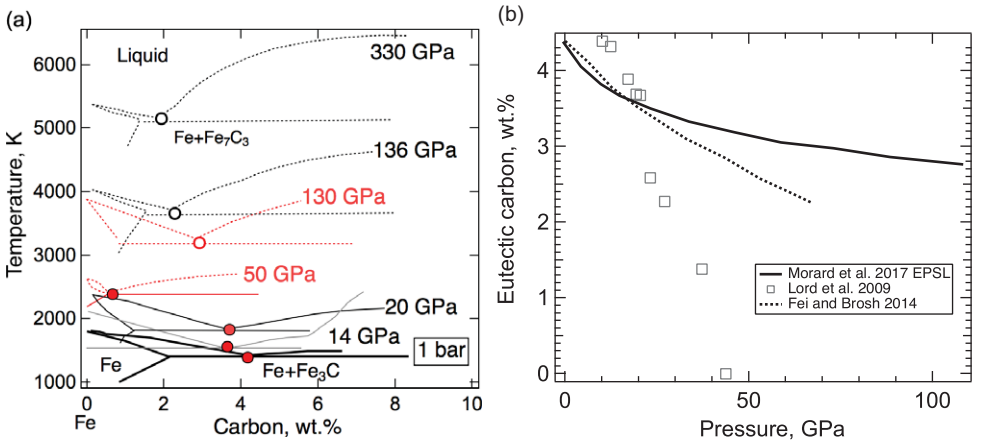

Figure 3.2 Fe–C binary system and eutectic composition. (a) Schematic phase diagram of the Fe–C binary system near the iron end member. 1 bar: thick black solid line,[17] 14 GPa: gray solid line,[18] 50 GPa and 130 GPa: red solid or dotted lines,[20] 20 GPa, 136 GPa, and 330 GPa: thick black solid or dotted lines.[22] Solid traces and filled circles are based on experimental measurements. Dotted traces and open circles are based on calculations and/or extrapolations. (b) Carbon content of the Fe–C eutectic liquid as a function of pressure.

only if the core composition is on the Fe-rich side of the eutectic point. Moreover, the light element contents of the solid and liquid must be sufficiently high and different to match the density contrast. If the eutectic composition is below 1 wt.%, it is unlikely to find a binary Fe–C composition with 5% density contrast between coexisting solid and liquid. It follows that carbon alone is unable to account for the density contrast at the ICB. The presence of sulfur and/or oxygen could help if they partition more strongly into the liquid phase. If the eutectic carbon content is as high as 3 wt.%, then a match by an Fe–C binary composition is possible (Figure 3.2).

Fe–L binary phase relations at 1 bar differ according to the nature of the light element, as is known from the metallurgy literature.[26] The phase relations at pressure and temperature conditions relevant for Earth's core are drastically different from those at 1 bar (Figure 3.3).

The Fe–S binary exhibits eutectic behavior between Fe and FeS at 1 bar and the sulfur content of the eutectic decreases with pressure (Figure 3.3). At core pressures, we may expect that a eutectic liquid containing <10 wt.% sulfur coexists with a solid with slightly less sulfur.[23,29,31,32] Therefore, sulfur alone cannot explain the density contrast at the ICB. At least 1–2 wt.% sulfur is likely to be present in the liquid core in addition to carbon and may enhance the stability of carbides or Fe–C alloys on the liquidus.[9]

The Fe–Si binary shows a narrow melting loop and only slight enrichment of silicon in the liquid at pressures up to 120 GPa (Figure 3.3). The eutectic composition contains 25 wt.% silicon at 21 GPa pressure[33] and <10 wt.% silicon at 80 GPa or higher,[34] and falls below 1.5 ± 0.1 wt.% at 127 GPa pressure.[30] Such a silicon-poor eutectic composition implies that FeSi may be a candidate for the inner core. Because Si stabilizes the

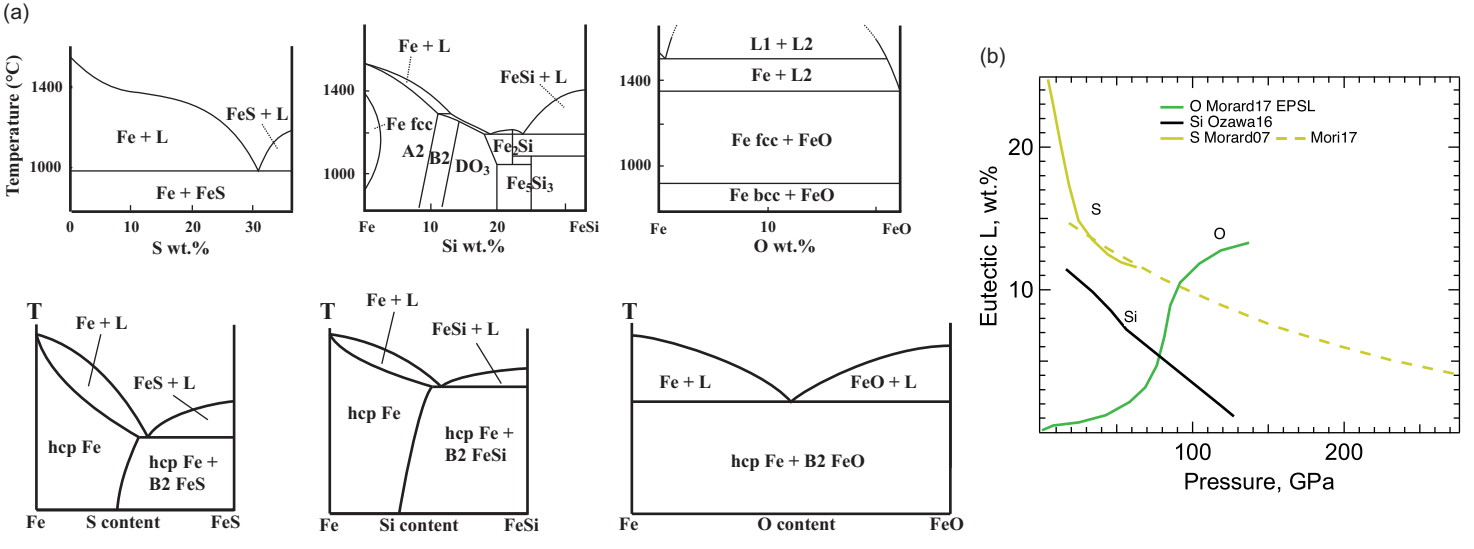

Figure 3.3 Fe–S, Fe–Si, and Fe–O binary phase diagrams and eutectic compositions. (a) Phase diagrams on the Fe-rich side of Fe–S, Fe–Si, and Fe–O systems at 1 bar (upper) and 330 GPa (lower).[27] (b) Eutectic composition as a function of pressure.
Data sources are Refs. 21 and 28–30. bcc = body-centered cubic.

body-centered cubic (bcc) structure, the inner core may be hcp Fe alloyed with Si or a mixture of a Si-rich bcc phase and a Si-poor hcp phase.[35,36] On the other hand, the silicon-poor eutectic composition and the nearly equal partitioning of silicon between solid and liquid iron at the ICB pressure[23,37] imply that silicon alone cannot explain the ICB density contrast.

While oxygen is a leading candidate for the light element in the liquid outer core, little oxygen is expected to be present in the solid inner core. At 1 bar, the Fe–O binary is characterized by a vast liquid miscibility gap.[26] At core pressures, the Fe–O system is more likely to be a eutectic with nearly pure Fe coexisting with Fe–O liquid (Figure 3.3). The eutectic oxygen content increases with pressure and exceeds 10 wt.% at >100 GPa.[21] Given its low solubility in solid Fe, the amount of oxygen in the inner core is probably negligible, but oxygen is the best candidate to explain the density difference between the solid and liquid cores.

3.2.2 Constraints from Densities of Fe–C Alloys and Compounds

The presence of light elements in Earth's core was initially inferred from comparing the observed density of the core with the measured density of iron under corresponding conditions. The pressure of the core is well constrained by geophysical and seismological data.[4] The temperature profile of the core is more uncertain and bears at least ±500 K uncertainties.[38] Compared with pure iron or iron–nickel alloys at the core *P–T* conditions,[39–42] the core is lighter than pure iron by 5–8% in the liquid outer shell and by 2–5% in the solid inner sphere.[5,43–45]

A viable composition model of the core must account for the density deficits. This is a straightforward and effective test, but requires knowledge of the phase relation and EoS of relevant Fe alloys in solid and liquid states at multi-megabar pressures and temperatures exceeding 4000 K. A wide range of mixtures of iron with C, O, Si, and S have been proposed as possible constituents of the outer core, whereas the solid inner core is most likely an iron alloy or a compound of iron with one of the light elements,[1–3] and therefore the test is somewhat simpler for the inner core.

Stimulated by the suggestion that the density of Fe_3C should be close to the observed value of the inner core,[9] measurements and calculations of the densities and elastic properties of iron carbides have been carried out (Tables 3.1 and 3.2). First-principles simulations coupled with structure search algorithms have been used to predict the iron–carbon alloys that are likely to be stable at Earth's inner core conditions. The energetically competitive stoichiometry ranges from Fe:C of 3:1 to 1:1 and includes Fe_3C, Fe_7C_3, Fe_5C_2, Fe_2C, and FeC stoichiometry.[46,47]

3.2.2.1 Fe_3C

The natural form of Fe_3C (cementite) occurs in iron meteorites and is known as cohenite. The composition of synthetic Fe_3C ranges from C deficiency with 4.2 wt.% or 17 at.% C

Table 3.1 *Elasticity parameters for solid Fe–C alloys*

Composition (wt.% L)	ρ_0 (g cm^{-3})	K_0 (GPa)	K_0'	P (GPa)	T (K)	Method	Ref.
Density							
Fe_3C							
	7.70(1)	175(4)	5.2(3)	0–73	300	PXD	121
	7.70(1)	174(6)	4.8(8)	0–30	300	PXD	61
	8.03(1)	290(13)	3.76(18)	0–187	300	PXD	50
	7.67	167	6.7	0–35	300	PXD	49
fm Fe_3C[a]	7.68(1)	192(3)	4.5(1)	0–31	300–1473	PXD	63
pm Fe_3C		161(2)	5.9(2)	0–50	300	SXD	62
pm Fe_7C_3	7.68(1)	201(12)	8.0(1.4)	4–158	300	SXD	64
nm Fe_7C_3	7.75(2)	307(6)	3.2(1)	7–167	300	SXD	64
fm Fe_7C_3	7.62(1)	186(5)	6.9(2.2)	0–7	300	PXD	70
Nonlinear Fe_7C_3	7.59(2)	166(13)	4.9(1.1)	7–20	300	PXD	
pm Fe_7C_3	7.68(2)	196(9)	4.9(2)	20–66	300	PXD	
fm Fe_7C_3	7.61(1)	201(2)	4 (fixed)	0–18		PXD	
pm Fe_7C_3[b]	7.70(2)	253(7)	3.6(2)	18–72	300–1973	PXD	41
	V_0 (m/s)	V = a0 + a1•ρ					
V_P		a0	a1				
Fe bcc	5800						89
Fe_3C	5330–5140						122
	5890	–3990	1290	0–50	300	NRIXS	55
	6103(413)	–8671	1900	0–68	300	HERIX	123
		–1138	9823	60–153	300	NRIXS	54
Fe_7C_3		2160	660	70–154	300	NRIXS	69
V_S							
Fe bcc	3000						89
Fe_3C	3010–3030						122
	3050(70)	1450	240	0–50	300	NRIXS	55
				0–50	300– 1450	NRIXS	94
		–961	4429	60–153	300	NRIXS	54
Fe_7C_3		843	242	70–154	300	NRIXS	69

[a] Θ_0 = 490(120) K, γ_0 = 2.09(4), q = –0.1(3).

[b] Θ_0 = 920(14) K, γ_0 = 2.57(5), q = 2.2(5).

HERIX = high-energy-resolution inelastic X-ray scattering; NRIXS = nuclear resonant inelastic X-ray scattering; PXD = powder X-ray diffraction; SXD = single-crystal X-ray diffraction.

(roughly Fe_5C) to C excess with 8.8 wt.% or 31 at.% C (exceeding Fe_7C_3).[48] At 1 bar and 300 K, Fe_3C has an orthorhombic structure (Figure 3.4). Although metastable at ambient conditions, the crystal structure remains unchanged to 187 GPa at 300 K[49,50] and to 25–70 GPa and 2200–3400 K.[51] Upon heating at pressures above 145 GPa, Fe_3C decomposes into a mixture of solid orthorhombic Fe_7C_3 and hcp Fe, then melts incongruently above

Table 3.2 *Elasticity parameters for liquid Fe–L alloys*

Composition (%L)		ρ_0 (g cm^{-3})	K_0 (GPa)	K_0'	P (GPa)	T (K)	Method	Ref.
wt.%	at.%							
Fe								
		7.02	109.7(7)	4.66(4)		1811	Shockwave	[44]
		5.19(3)	24.6(6)	6.65(4)	50–350	7000	FPMD	[82]
Fe–S								
10	6	5.2	48.0(2.0)	4	0–6	1770	X-ray absorption	[124]
10		5.5	63	4.8	0–20	1773–2123	Sink–float	[125]
20	12.5	4.41	35(1)	4.9	0–8	1673	Ultrasonic	[96]
27	17.4	4.07	25(1)	5.3	0–8	1673	Ultrasonic	
30	19.7				0–5.4	1573–1673	Ultrasonic	[126]
11.7	7	6.28	83.7	4.98	150–300	4000	FPMD	[97]
		5.43	49.6	5.08		6000		
16	9.8	5.72	64.4	4.94		4000		
		5.06	42.9	5.02		6000		
Fe–C								
0–4	0–0.9	[a]			0	1523–1823	Sessile drop	[73]
3.5	0.8	6.91	83.9	5.9(2)	0–4	1700	Ultrasonic	[127]
		6.91	100(1)	6.2(6)		1700		
		7.02(1.5)	55.3(2.5)	5.2(1.5)	2–7	1500		
2.0–4.0	0.4–0.9		65.0	6.0	42	3000	X-ray diffraction	[66]
	10.9(4)							
	12.1(4)							
5.7	1.3		Similar to Tera10		0–5.4		X-ray absorption	[128]
			Larger		5.4–7.8			
3.9	16	6.51	110(9)	5.1(3)	7–70	2500	X-ray absorption	[65]
6.7	1.5	6.5	54(3)	4	0–10	1973	X-ray absorption	[129]
Fe–Si								
17	9.3	5.88	68(1)	4	0–12	1773	Sink–float	[130]
17		6.33	75	4	0–5	1650	X-ray absorption	[131]
Fe–O								
22	7.5	5.45	128	3.85		5000	Thermo	[132]
Fe–H								
0.8	0.01	6.2	82.4	4.79	125–200	4000	FPMD	[101]
		5.63	62.9	4.76		6000		
1.2	0.02	5.88	73.1	5.02		4000		
		5.23	53.2	4.82		6000		

[a] $\rho = 7.10 - 0.0732x - (8.28 - 0.874x)\bullet10^{-4}\bullet(T - 1823)$, x = wt.% C, T in K.

FPMD = first-principles molecular dynamics.

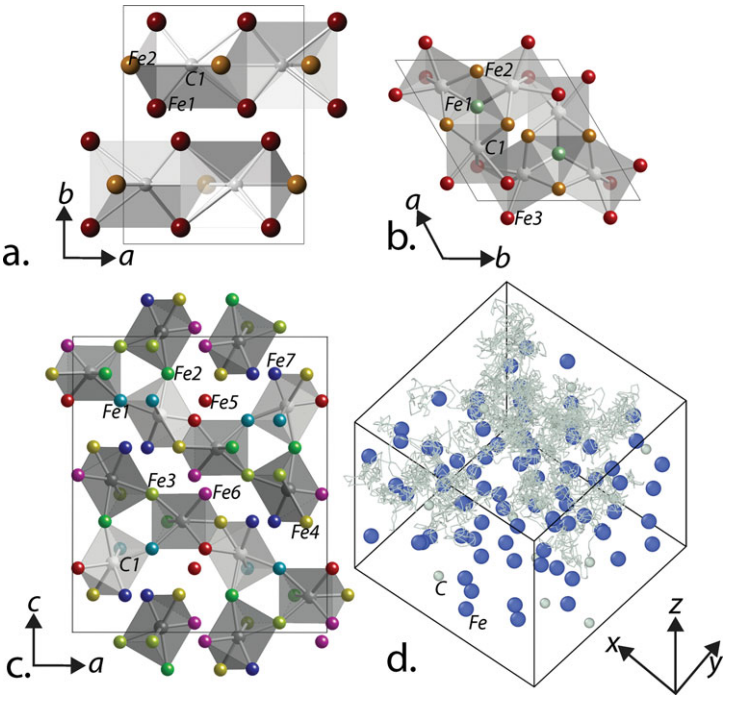

Figure 3.4 Atomic-scale structures of crystalline and molten iron carbide alloys. (a) Orthorhombic Fe_3C (space group Pnma), (b) hexagonal Fe_7C_3 (space group $P6_3mc$) and (c) orthorhombic Fe_7C_3 (space group Pbca). In both Fe_3C and Fe_7C_3 polymorphs, the fundamental building blocks are triangular prisms (CFe_6). Three such prisms are connected via shared vertices in a triangular arrangement (triads). The triads are stacked up along the c-axes for hexagonal polymorphs and along b-axes for orthorhombic polymorphs of Fe_7C_3. The carbon atoms are shown as gray spheres and the iron atoms are colored based on the distinct Wyckoff sites.[57,58] (d) A snapshot of a molten iron carbide alloy from molecular dynamics simulations. The computational supercell is shown and has orthogonal axes with $x = y = z$. The diffusion trajectory of a carbon atom is shown for reference.

3400 K.[52] Cementite is ferromagnetic at ambient conditions and its Curie temperature is sensitive to small deviations from stoichiometry.[53] It undergoes ferromagnetic to paramagnetic transition and spin-pairing transition at high pressures.[54–56]

The density of Fe_3C at ambient conditions is 2.5% smaller than that of fictive hcp iron, corresponding to ~1.4% density reduction for 1 wt.% carbon (i.e. a compositional expansion coefficient α_c of 1.4).[59] Pressure-induced magnetic transitions lead to abrupt but small reductions in density and/or compressibility.[54,55,57,60] The calculated density of Fe_3C at the ICB pressure and 300 K is comparable to that of the inner core, but too low when thermal expansion is considered (Figure 3.5). A more appropriate test requires knowledge of the thermoelastic parameters of the non-magnetic phase.

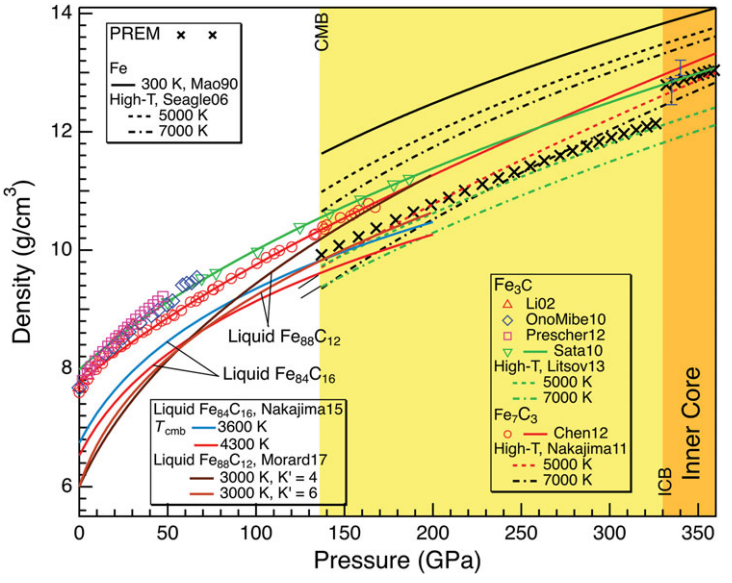

Figure 3.5 Density of Fe–C alloys and compounds as a function of pressure of iron carbides. CMB = core–mantle boundary. Preliminary reerence Earth model (PREM): black crosses;[4] hcp Fe at 300 K: black solid curve;[40] hcp Fe at 5000–7000 K calculated using the Mie–Grüneisen–Debye EoS.[42] Fe_3C at 300 K;[49,50,61,62] Fe_3C at 5000–7000 K.[63] Fe_7C_3 at 300 K;[64] Fe_7C_3 at 5000–7000 K.[41] Uncertainties are shown as error bars.[64] Liquid with $Fe_{84}C_{16}$ compoisition.[65] Liquid with $Fe_{88}C_{12}$ composition.[66]

3.2.2.2 Fe_7C_3

The metallurgical form of Fe_7C_3, known as Eckström–Adcock carbide, adopts a hexagonal structure at 1 bar and 300 K (Figure 3.3). An orthorhombic structure is also observed and may be stabilized with silicon impurities.[67] Non-stoichiometry is also observed in Fe_7C_3 and ranges from 8.0 to 10.8 wt.% (29–36 at.%) C, where the C-excess end member exceeds Fe_2C stoichiometry.[48] The crystal structure of Fe_7C_3 remains stable up to 185 GPa and 5200 K,[52,68] but it undergoes pressure-induced magnetic transitions.[18,69–71] At ambient conditions, the compositional expansion coefficients of h-Fe_7C_3 (~1.0) is smaller than that of Fe_3C (~1.4). The calculated density of the non-magnetic Fe_7C_3 is broadly consistent with that of the inner core at the relevant pressures and temperatures, thus supporting the carbide inner core model (Figure 3.5).

3.2.2.3 Fe–C Alloy Near the Iron End Member

In the simplified Fe–C model, the inner core may consist of an Fe–C alloy rather than a carbide.[22] The Fe–C alloy would contain no more than 1 wt.% carbon according to geochemical considerations and the measured solubility of carbon at pressures greater than 40 GPa.[20,21] However, 1.0–2.5 wt.% carbon may not be sufficient to reproduce the density deficit of the inner core[72] and hence would require the presence of other light elements.

3.2.2.4 Liquid Fe–C Alloy

A carbide inner core implies that the liquid outer core contains more carbon than the eutectic composition at relevant pressures (Figure 3.2). Even if the solid inner core is not made of carbides, a substantial amount of carbon may still be present in the liquid outer core, which occupies more than 90% of the core by mass or volume.

At ambient pressure, adding 1.3–2.8% carbon only reduces the density of liquid Fe by ~1% (α_c = 0.4–0.8).[73] Experimental measurements of an Fe liquid with 2.8 wt.% carbon suggest an α_c of 2–4 at the core–mantle boundary (CMB) pressure of 136 GPa and 3000 K,[66] which is in broad agreement with the calculated value of 1.3,[74] considering uncertainty and extrapolation. The larger α_c values at core pressures are consistent with Fe–C liquid being less compressible than Fe liquid.[65] Even with α_c = 2–4, 1.8–2.7 wt.% carbon is needed to explain the 5–8% density deficit in the outer core. This is higher than the upper limit from cosmochemical and geochemical considerations; hence, carbon cannot be the sole light element in the outer core.

3.2.2.5 Other Light Elements

All candidate light elements have been shown to reduce the density of solid Fe (Figure 3.6). The fitted compositional expansion coefficients of light elements in solid Fe alloys are comparable to the calculated results for liquid Fe alloys.[74] On the per wt.% basis, carbon may be slightly more efficient than O, Si, and O at reducing the density of iron, and therefore a slightly smaller amount is needed to account for the 5–8% density deficit in the outer core (Table 3.3). Combinations of light element such as that of sulfur and silicon[75] are found to satisfy the density constraints.

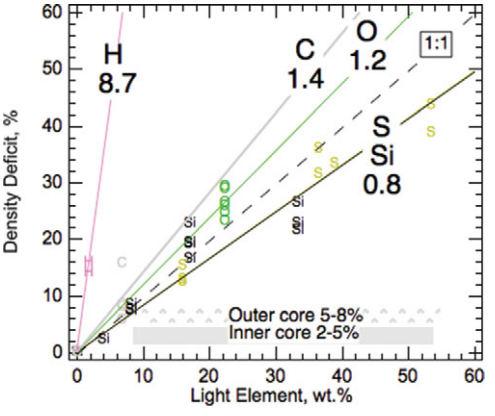

Figure 3.6 Compositional expansion coefficients of light elements in solid iron alloys. The values are derived from fits to solid Fe–L alloys and compounds.[3]

Table 3.3 *Compositional expansion coefficients*

	Solid[a]	Liquid at CMB[b]	Liquid at ICB[b]	LE, wt.%[c]	LE, wt.%[d]
H	8.7	–	–	0.6	0.9
C	1.4	1.3	1.3	4	6
O	1.2	1.1	1.0	4	7
Si	0.8	0.7	0.6	6	10
S	0.8	0.8	0.7	6	10

Compositional expansion coefficient is defined as the relative amount of density reduction per wt.% light element.[59]

[a] Li and Fei.[3]

[b] Badro et al.[74]

[c] Amount of light element needed to account for 5% density deficit in the outer core.

[d] Amount of light element needed to account for 8% density deficit in the outer core.

LE = light element.

3.2.3 Constraints from Sound Velocities of Fe–C Alloys and Compounds

Comparison between the preliminary reerence earth model (PREM) and iron reveals a prominent mismatch in the shear wave velocity, V_S, between the inner core and Fe or Fe–Ni alloys at corresponding pressures and 300 K (Figure 3.7). The discrepancy cannot be explained by the effect of temperature alone[76–78] and has been attributed to partial melting,[79] strong pre-melting effects,[80,81] and/or the presence of light elements.[55] In contrast, the compressional wave velocity, V_P, in the inner core is broadly consistent with that of hcp Fe (Figure 3.7). In the outer core, the bulk sound velocity may be comparable to or as much as 4% higher than liquid iron at corresponding conditions.[43,82] The presence of light elements, therefore, should not significantly affect the V_P of iron for this match to hold.

The sound velocities in the core increase linearly with density, following Birch's law (Figure 3.7). The velocity–density relations of solid and liquid Fe are consistent with Birth's law, but for solid Fe the V_P slope at 300 K or along a Hugoniot is steeper than that of the core. For V_S, deviation from Birch's law behavior was predicted by theory[83] and observed at high temperatures,[77] although this is not resolved in all studies.[84] A candidate Fe–L alloy must reproduce the velocity gradients in the core.

The speed of sound traversing the inner core is anisotropic by 3–4% in V_P and ~1% in V_S.[85,86] The anisotropy in sound speed may reflect convective alignment of anisotropic hcp Fe crystals[87] or an Fe–L alloy.[88] A candidate inner core phase needs to exhibit large enough elastic anisotropy to match the observations.

3.2.3.1 Fe_3C

As a candidate for the inner core phase, Fe_3C stands out in terms of its potential to account for the observed anisotropy. If the measured and calculated strong anisotropy in the sound

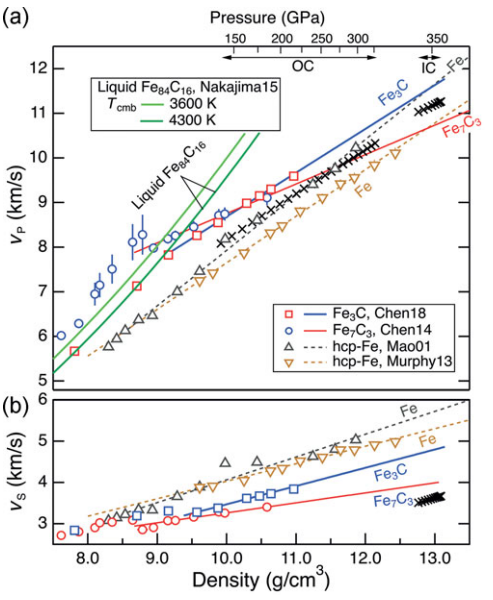

Figure 3.7 Sound velocity of Fe–C alloys and compounds. V_P and V_S of Fe carbides and liquid Fe–C as a function of density. Data are from Refs. 54, 65, 69, 89, and 90. The velocities of Fe–Ni alloys (not shown)[91] are similar to that of Fe. The top axis denotes the pressure range of the outer core (OC) and inner core (IC) according to the density–pressure relationship in PREM.

velocity of Fe_3C at ambient conditions[92,93] is applicable at core conditions, then only a small degree of alignment would be needed for Fe_3C to match the observations.

Existing data suggest that Fe_3C may provide a good match for the V_S in the inner core. At ambient conditions, the V_S of Fe_3C is similar to that of bcc Fe (Table 3.1). At 300 K, a magnetic transition near 5 GPa leads to a reduction in the V_S and its Birch's law slope so that the extrapolated V_S of Fe_3C at the inner core pressure is much smaller than that of hcp Fe and closer to the core values.[55] The high-spin to low-spin transition near 50 GPa leads to a further decrease in the Birch's law slope.[54] Moreover, at high temperatures, the V_S of Fe_3C deviates from Birch's law behavior toward the inner core values; hence, it can potentially explain the anomalously low V_S in the inner core without invoking partial melt or strong pre-melting effects.[94]

A potential match in V_P is also consistent with existing data. The range of measured V_P of Fe_3C at 1 bar and 300 K encompasses that of bcc Fe (Table 3.1). The magnetic transition to the paramagnetic phase of Fe_3C results in elastic softening and a shallower Birch's law slope of V_P, whereas the paramagnetic to non-magnetic transition does not seem to produce a visible effect.[54] At 300 K and inner core pressures, the extrapolated V_P of Fe_3C is higher than that of the inner core (Figure 3.7). A close match is possible if V_P at high temperature is lowered by a suitable amount as a result of deviation from Birch's law.

3.2.3.2 Fe_7C_3

The most compelling support for an Fe_7C_3 inner core comes from its ability to match the anomalously low V_S and high Poisson ratio, in addition to reproducing the density deficit.[58,69] While the ferro- to para-magnetic transition at 7.0–7.5 GPa does not seem to have obvious effect on sound velocities, significant shear softening accompanies the magnetic collapse at 40–50 GPa, resulting in pronounced reductions in V_P, V_S, and their Birch's law slopes (Figure 3.7). At pressures relevant to Earth's inner core, the extrapolated value of V_S of Fe_7C_3 at 300 K is only slightly higher than the observed value. There is likely a good match for V_S after considering further reduction at high temperature. It remains to be tested whether Fe_7C_3 can simultaneously match V_S, V_P, and anisotropy.

3.2.3.3 Fe–C Alloy Near the Iron End Member

First-principles calculations show that adding 1.0–2.5 wt.% carbon into the hcp Fe crystal structure increases its V_P and decreases its V_S, and this would help explain the observed anisotropy in compressional wave velocities, although there is a mismatch in shear wave anisotropy.[72]

3.2.3.4 Liquid Fe–C Alloy

Adding carbon increases the V_P of liquid iron (Table 3.1). For 1 at.% carbon, the average effect is 0.2% at 1 bar. It may increase to an estimated value of 0.8–1.2% at the core conditions, presumably because liquid Fe–C is less compressible than liquid Fe,[65] or remains at 0.2% at high pressures and high temperatures.[74] In any case, the V_P of an Fe–C alloy with <1 wt.% carbon would be consistent with the observed value in the outer core.

3.2.3.5 Other Light Elements

The sound velocities of other Fe–L alloys remain poorly constrained (Figure 3.8 and Table 3.4). The effect of sulfur on the sound velocities is not yet sufficiently understood to allow firm tests of Fe–S models for the core.[28,74,95–98] Further studies are needed to

Table 3.4 *Melting curve parameters of Fe–L alloys*

	a	c	P_0 (GPa)	T_0 (K)	T_{eut} CMB (K)	X_{eut} CMB (at.%)	dT/dx (K/at.%)
Fe–C	8.5	3.8	0	1420	2990(200)	11(5)	110(80)
Fe–O	17	3.8	0	1800	3200(200)	30(3)	33(11)
Fe–18 wt.% Si	23.6	1.89	0	1600	–	4	–
Fe–S	10.5	3	21	1260	2870(200)	15(5)	89(56)

The parameters are fitted to the Simon–Glatzel equation $(T_m/T_{m0})^c = (P_m - P_{m0})/a$. Data are from Morard et al.[75]

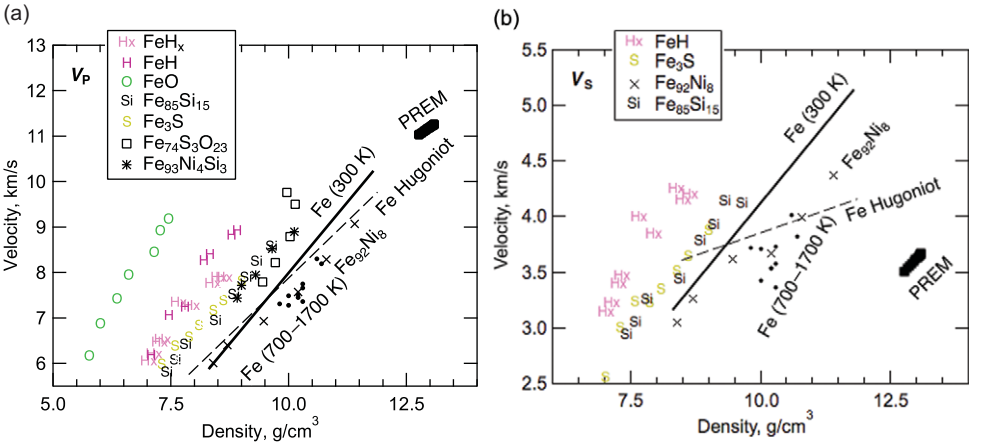

Figure 3.8 Sound velocities of Fe–H, Fe–O, Fe–S, and Fe–Si alloys and compounds. Compressional wave velocity V_P (a) and shear-wave velocity V_S (b) versus density relations. PREM;[4] hcp Fe at 300 K: solid line;[89] hcp Fe at temperatures between 700 and 1700 K: solid circles;[77] Fe from shockwave experiments: dashed line;[76] $Fe_{92}Ni_8$ at 300 K: crosses;[91] Fe_3S at 300 K;[102] $Fe_{85}Si_{15}$ at 300 K;[91] FeO at 300 K;[103] FeH_x at 300 K;[104] FeH at 300 K;[105] $Fe_{74}S_3O_{23}$ from shockwave experiments;[106] $Fe_{93}Ni_4Si_3$ at 300 K.[107]

resolve the disagreements concerning oxygen as a major light element in the core.[74,99] Computations suggest that an Fe–H alloy with 1 wt.% H can reproduce the density and V_P of the liquid outer core and therefore could be the primary alloy element, but Fe–H alloys cannot reproduce the V_S of the inner core.[100,101]

3.2.4 Constraints from Melting Temperatures of Fe–C Alloys

An independent constraint on the carbon content of the outer core can be obtained from the melting temperatures of iron alloys (Figure 3.8). The outer core is entirely molten, whereas the base of the mantle is mostly solid;[108] hence, the melting temperature of a candidate Fe–C alloy must be lower than the solidus of overlying mantle at the CMB pressure. In addition, as the geotherm is expected to follow an adiabat, which has a smaller dT/dP slope than the melting curve, the temperature at CMB is expected to be 400–900 K lower than its crystallization temperature at the ICB.[38,45]

The solidus temperature at the CMB is estimated at 4100–4200 K for peridotitic composition.[109] For comparison, core temperature profiles for pure Fe or Fe–Ni alloys would lead to a temperature at the CMB of 5400–5900 K,[38] which clearly exceeds the upper bounds on the mantle side (Figure 3.9); thus, these compositions are incompatible with a molten iron alloy and solid silicate coexisting at the CMB.

Carbon reduces the melting point of iron. Using linear interpolation between pure Fe and the eutectic liquid, the melting point reduction is estimated at >100 K per at.% carbon

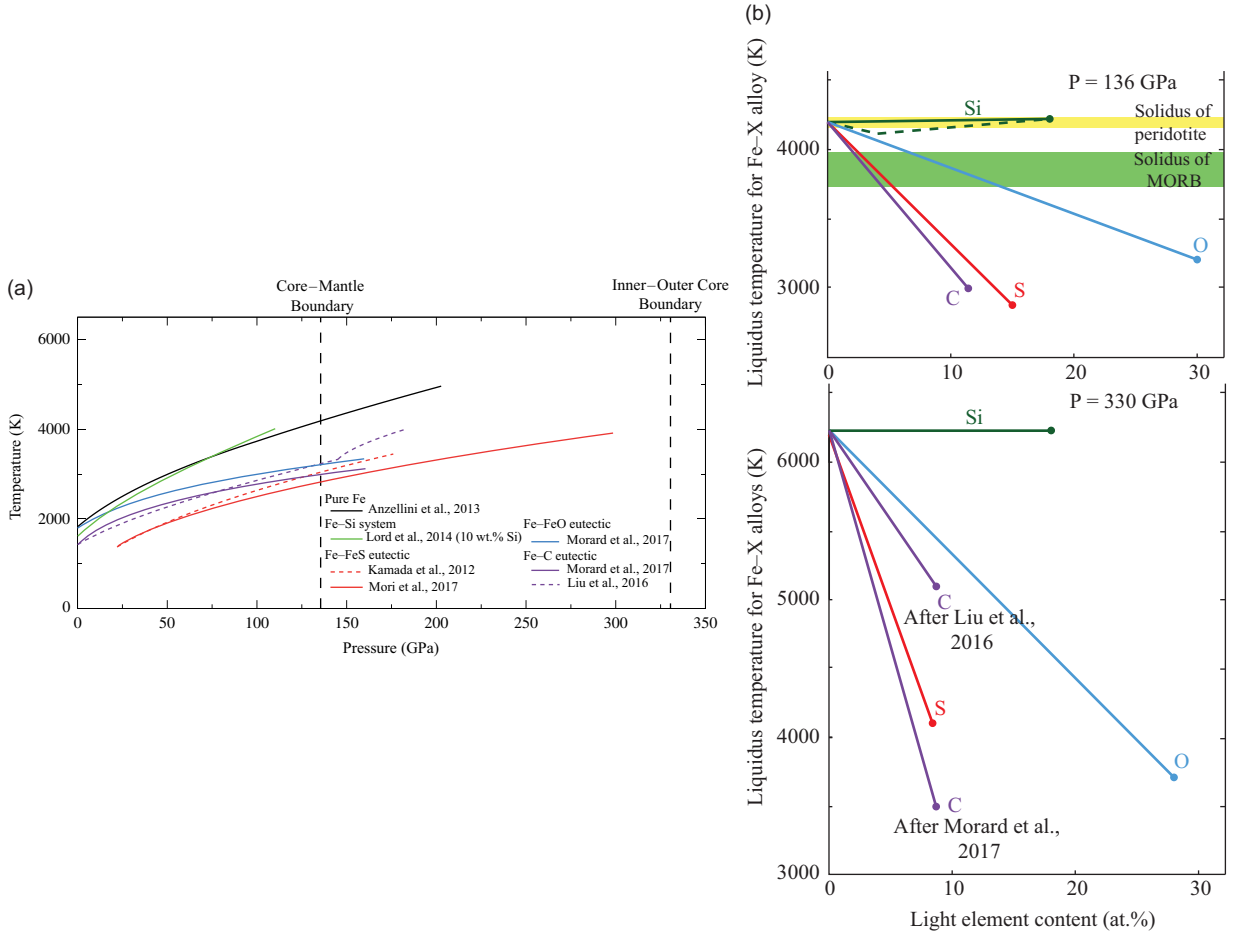

Figure 3.9 Melting temperatures of Fe-rich alloys. (a) Melting curves of pure iron,[38] and Fe–10 wt.% Si[110] and eutectic melting curves of Fe–Fe_3S (dashed line,[31] solid line[29]), Fe–FeO,[21] and Fe–Fe_3C (dashed line,[111] solid line[21]). The different melting curves are represented over the pressure range at which experiments were performed without any extrapolation. Pressures for the CMB and ICB are indicated by thick vertical dashed lines. (b, top) Liquidus temperatures in Fe–X systems compared with melting temperatures of mantle materials at the CMB (136 GPa), represented as linear interpolations between the melting point of pure Fe[38] and the eutectic compositions.[21] Solidi at CMB pressure for the peridotitic[109] and mid-ocean ridge basalt mantle[112] are represented by horizontal bands. (b, bottom) Extrapolated liquidus under ICB pressure for sulfur,[29] oxygen,[21] silicon,[110] and carbon.[21,52]

at 136 GPa.[21] At the ICB pressure, the melting point reduction effect of carbon may be similar to that at the CMB[52] or as much as 350 K/at.%.[21]

Experimentally determined eutectic melting temperatures agree within 150 K for the Fe–S, Fe–Si, and Fe–O systems.[3,21,30] Adding 1 at.% C, O, Si, and S to liquid iron reduces its melting point by 100 K for C and S, 50 K for O, and <30 K for Si at the pressure of the CMB (Figure 3.8). To pass the physical state test, a core with a single light element must contain at least 5 at.% S or C, or at least 15 at.% O.[29] The melting points of Fe–Si alloys are too high and therefore silicon cannot be the only light element in the outer core. The presence of other light elements such as carbon, oxygen, and/or sulfur are required to lower its crystallization temperature.

Compositions containing two or more lighter elements exhibit more complex behavior. While the alloying effect of oxygen on the eutectic point of the Fe–S system was found to be minor,[113] shock experiments at 100–200 GPa estimated that the presence of 8 wt.% (2.4 at.%) oxygen and 2 wt.% (1.2 at.%) sulfur would reduce the melting point of iron by 600 K.[106,114] This is more than twice the combined reductions of oxygen (120 K) and sulfur (120 K), suggesting non-ideal mixing in the ternary system.

3.3 Implications of Carbon as a Major Light Element in the Core

If the inner core consists of Fe_7C_3 with 8.41 wt.% carbon, the average concentration of carbon in the core would be at least ~0.3 wt.%, implying that the core has nearly one order of magnitude more carbon than the total amount in the surface reservoirs and silicate Earth, and hence it is by far the largest carbon reservoir in Earth (Figure 3.1). The bulk Earth would contain 0.1 wt.% carbon, higher than the estimated 0.03 wt.% for a half-mass condensation temperature of 40 K.[7,115] This result would question the validity of the volatility trend for highly volatile elements such as carbon.

Recent experiments show that Fe_7C_3 exhibits the highest electrical resistivity among all Fe–L alloys.[116] As a major element in the core, carbon may influence the thermal transport properties of the core, with implications for the evolution of the geodynamo.

3.4 Carbon in the Core Over Time

Carbon may move across the CMB over geological time if chemical disequilibrium was introduced during Earth's accretion or subsequent evolution. Earth's core may have been initially out of equilibrium with the mantle,[117] or the silicate Earth may have acquired most of its highly volatile elements through a late veneer.[118] Furthermore, chemical equilibrium at the CMB may have been perturbed as a result of secular cooling or inner core growth, which may have enriched or depleted carbon in the outer core depending on the carbon partitioning between the solid and liquid (Figure 3.2). Experiments suggest that mobility of carbon along grain boundaries may allow its transport over geologically significant length scales of 10 km over the age of Earth.[119] Facilitated by mantle convection, rapid

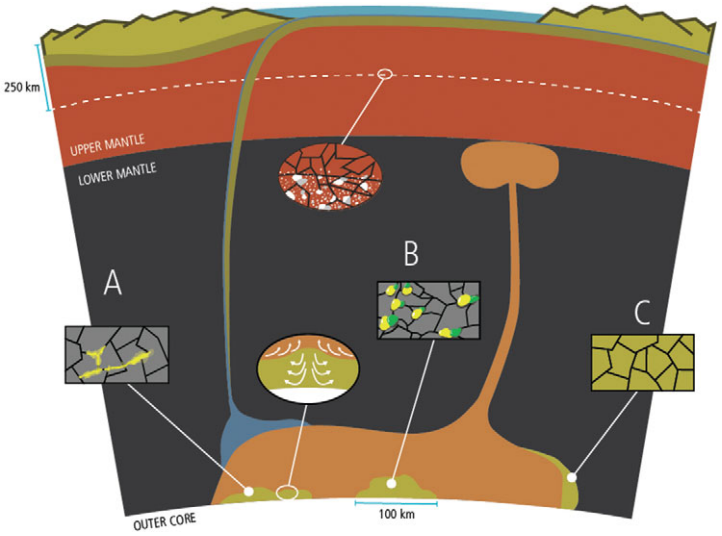

Figure 3.10 Carbon transport from subducted slabs to Earth's core. Schematic illustration of slab-derived Fe–C melt bringing carbon from Earth's surface to the core, modified after Liu et al.[111] The upper oval-shaped balloon shows elemental carbon or iron carbides (gray) associated with metallic iron (white) in the mantle at depths greater than 250 km. Three rectangular boxes represent Fe–C melts at the base of the mantle (heights are exaggerated): (a) Fe–C melt (yellow) that wets the solid silicate matrix (gray); (b) non-wetting Fe–C melt (yellow) coexisting with a small degree of silicate melt (green) in a solid silicate matrix (gray); and (c) solid phases (yellow–gray) that have become iron rich through reaction with the Fe–C melt. The lower oval-shaped balloon indicates dynamic stirring, which may prevent or slow down the draining of dense Fe–C melts to the core.

grain-boundary diffusion may have brought core-derived carbon to Earth's surface and thus connected the billion-year deep carbon cycle to the near-surface million-year shallow carbon cycle.

Ongoing carbon sequestration by the core may have resulted from subduction of the hydrothermally altered oceanic lithosphere carrying carbonates and organic matter into the deep Earth. While $CaCO_3$ in slabs may have been preserved under reducing lower-mantle conditions, the $MgCO_3$ component could have been destabilized by metallic iron-form diamonds or iron carbides.[120] Slab-derived Fe–C mixtures are expected to partially melt in the D′′ layer.[111] The melt may have accumulated near the CMB over time and episodically drained into the core (Figure 3.10).

3.5 Conclusion

We have evaluated constraints on the carbon budget of Earth's core by comparing the density, velocity, and elastic anisotropy of Fe–C alloys and compounds at core conditions with seismic observations. Existing data support the model of the inner core consisting of

iron carbide Fe_7C_3, which could solidify from an Fe–C–S liquid core containing up to 1 wt. % carbon. Fe_7C_3 is unique in its ability to match the anomalous V_S and high Poisson ratio of the inner core. Its density and V_P are also broadly consistent with the PREM, but need to be further tested against the anisotropy observations. On the contrary, Fe_3C seems unstable and too light to match the inner core density. Given the upper limit of 1 wt.% carbon in the core, an Fe–C alloy is unable to generate the observed density deficit in the inner core.

The presence of 1 wt.% carbon in the outer core provides a good match to the V_P and is consistent with the coexistence of a molten iron alloy with solid silicate at the CMB. However, 1 wt.% carbon is insufficient to account for the density deficit in the outer core and cannot reproduce the density contrast at the ICB, and therefore other light elements such as H, O, S, or Si must be present in the outer core.

Earth's core remains potentially by far the largest carbon reservoir of the planet. It may participate in the long-term global carbon cycle through carbon transport across the CMB via grain-boundary diffusion, mantle convection, and sequestering slab-derived Fe–C melts.

The outer core likely contains multiple light elements. At least 1–2 wt.% sulfur is likely to be present in the outer core and would help account for its density deficit and the core's largely molten state. Oxygen may be required in the liquid outer core to explain the density contrast at the ICB, although the amount of oxygen remains uncertain. Silicon does not help explain the density contrast across the ICB or the coexistence of the liquid core with the overlying solid mantle. Existing data are insufficient to resolve the competing models of core composition because of limited data coverage in the relevant pressure–temperature–composition space and uncertainties in experimental measurements and theoretical simulations. Future studies should focus on expanding the experimental data range and investigating complex systems that contain more than one light element.

3.6 Limits to Knowledge and Unknowns

Earth's core is potentially by far the largest carbon reservoir of the planet. To assess the role of the core in Earth's deep carbon cycle, we need to test the hypothesis of iron carbide as the dominant component of the solid inner core and quantify the carbon content of the liquid outer core. In the past decade, research in deep carbon has significantly improved our knowledge of the physical properties and melting behavior of carbon-bearing iron alloys at the extreme pressure and temperature conditions in the deep Earth. Limits to our knowledge mainly stem from incomplete data coverage for the relevant pressures, temperatures, and compositions. For simplified compositions, the properties of liquid iron or iron alloys are still limited to relatively low pressures and temperatures far below the relevant ranges of the core. Investigations of complex iron alloys containing nickel and two or more light elements have only covered small subsets of the entire plausible pressure–temperature–composition space. Effects of temperature on the magnetic transitions and elasticities of solid iron alloys remain poorly constrained. Direct measurements of the densities and velocities of solids at inner core pressures are not yet available.

Acknowledgments

The authors thanks Rajdeep Dasgupta, James Badro, an anonymous reviewer, and Dave Walker for providing critical comments and constructive suggestions. JL acknowledges NSF EAR-1763189, NSF AST-1344133, and Sloan Foundation Deep Carbon Observatory Grant G-2017-9954. BC acknowledges NSF EAR-1555388 and NSF EAR-1565708. MM acknowledges XSEDE resources, NSF EAR-1634422, and NSF EAR-1753125.

Questions for the Classroom

1 How do researchers infer the presence of volatile elements such as carbon in Earth's liquid outer core?
2 As a candidate for the principal light element in Earth's core, what are the strongest arguments for and against carbon?
3 What is the plausible range of carbon content in Earth's core, and how do we know this?
4 Why was an iron carbide proposed as a candidate for the dominant component of Earth's solid inner core? How can we test this hypothesis?
5 Why is the knowledge of the eutectic composition of binary systems Fe–X, where X is an element lighter than iron such as hydrogen, carbon, oxygen, silicon, or sulfur, important for constraining Earth's core composition?
6 How do pressure and temperature affect magnetism in iron-rich alloys?
7 What are "spin-pairing" or "high-spin to low-spin" transitions in iron-rich alloys?
8 How is the elasticity of an iron alloy affected by pressure-induced magnetic transition?
9 How do light elements such as carbon affect the thermodynamic stability of iron–nickel alloys?

References

1. Jeanloz, R., The nature of the Earth's core. *Annu Rev Earth Planet Sci*, **18**, 357–386 (1990). doi:10.1146/annurev .ea.18.050190.002041
2. Poirier, J.P., Light elements in the Earth's outer core: a critical review. *Phys Earth Planet Inter*, **85**, 319–337 (1994). doi:10.1016/0031-9201(94)90120-1
3. Li, J. & Fei, Y., Experimental constraints on core composition. In *Treatise on Geochemistry, Vol*, eds. H.D. Holland & K.K. Turekian (Amsterdam: Elsevier Ltd., 2014), pp. 521–546.
4. Dziewonski, A.M. & Anderson, D.L., Preliminary reference Earth model. *Phys Earth Planet Inter*, **25**, 297–356 (1981). doi:10.1016/0031-9201(81)90046-7
5. Birch, F., Elasticity and constitution of the Earth's interior. *J Geophys Res*, **57**, 227–286 (1952). doi:10.1029/JZ057i002p00227
6. Jarosewich, E., Chemical analyses of meteorites – a compilation of stony and iron meteorite analyses. *Meteoritics*, **25**, 323–337 (1990). doi:10.1111/j.1945-5100.1990.tb00717.x
7. McDonough, W.F., Compositional model for the Earth's core, in *Treatise on Geochemistry, Vol. 3*, eds. H.D. Holland & K.K. Turekian (Oxford: Elsevier Ltd., 2014), pp. 559–576.

8. Dasgupta, R. & Walker, D., Carbon solubility in core melts in a shallow magma ocean environment and distribution of carbon between the Earth's core and the mantle. *Geochim. Cosmochim. Acta*, 72, 4627–4641 (2008). doi:10.1016/j.gca.2008.06.023
9. Wood, B.J., Carbon in the core. *Earth Planet Sci Lett*, **117**, 593–607 (1993). doi:10.1016/0012-821X(93)90105-I
10. Wang, C., Hirama, J., Nagasaka, T., & Ban-Ya, S., Phase equilibria of liquid Fe–S–C ternary system. *ISIJ Int*, **31**, 1292–1299 (1991). doi:10.2355/isijinternational.31.1292
11. Chi, H., Dasgupta, R., Duncan, M.S., & Shimizu, N., Partitioning of carbon between Fe-rich alloy melt and silicate melt in a magma ocean – implications for the abundance and origin of volatiles in Earth, Mars, and the Moon. *Geochim Cosmochim Acta*, **139**, 447–471 (2014). doi:10.1016/j.gca.2014.04.046
12. Dalou, C., Hirschmann, M.M., von der Handt, A., Mosenfelder, J., & Armstrong, L.S., Nitrogen and carbon fractionation during core–mantle differentiation at shallow depth. *Earth Planet Sci Lett*, **458**, 141–151 (2017). doi:10.1016/j.epsl.2016.10.026
13. Li, Y., Dasgupta, R., & Tsuno, K., The effects of sulfur, silicon, water, and oxygen fugacity on carbon solubility and partitioning in Fe-rich alloy and silicate melt systems at 3 GPa and 1600 C. *Earth Planet Sci Lett*, **415**, 54–66 (2015). doi:10.1016/j.epsl.2015.01.017
14. Tsuno, K., Grewal, D.S., & Dasgupta, R., Core–mantle fractionation of carbon in Earth and Mars: the effects of sulfur. *Geochim Cosmochim Acta*, **238**, 477–495 (2018). doi:10.1016/j.gca.2018.07.010
15. Wood, B.J., Li, J., & Shahar, A., Carbon in the core: its influence on the properties of core and mantle. *Rev Mineral Geochem*, **75**, 231–250 (2013). doi:10.2138/rmg.2013.75.8
16. Dasgupta, R., Ingassing, storage, and outgassing of terrestrial carbon through geological time, in *Carbon in Earth*, eds. R.M. Hazen, A.P., Jones, & J.A. Baross (Washington, DC: Mineralogical Society of America, 2013), pp. 183–229.
17. Chipman, J., Thermodynamics and phase diagram of the Fe–C system. *Metall Trans*, **3**, 55–64 (1972). doi:10.1007/BF02680585
18. Nakajima, Y., Takahashi, E., Suzuki, T., & Funakoshi, K.I., "Carbon in the core" revisited. *Phys Earth Planet Inter*, **174**, 202–211 (2009). doi:10.1016/j.pepi.2008.05.014
19. Hirayama, Y., Fujii, T., & Kei, K., The melting relation of the system iron and carbon at high pressure and its bearing on the early stage of the Earth. *Geophys Res Lett*, **20**, 2095–2098 (1993). doi:10.1029/93GL02131
20. Lord, O.T., Walter, M.J., Dasgupta, R., Walker, D., & Clark, S.M., Melting in the Fe–C system to 70 GPa. *Earth Planet Sci Lett*, **284**, 157–167 (2009). doi:10.1016/j.epsl.2009.04.017
21. Morard, G. et al., Fe–FeO and Fe–Fe–C melting relations at Earth's core–mantle boundary conditions: implications for a volatile-rich or oxygen-rich core. *Earth Planet Sci Lett*, **473**, 94–103 (2017). doi:10.1016/j.epsl.2017.05.024
22. Fei, Y. & Brosh, E., Experimental study and thermodynamic calculations of phase relations in the Fe–C system at high pressure. *Earth Planet Sci Lett*, **408**, 155–162 (2014). doi:10.1016/j.epsl.2014.09.044
23. Alfè, D., Gillan, M.J., & Price, G.D., *Ab initio* chemical potentials of solid and liquid solutions and the chemistry of the Earth's core. *J. Chem Phys*, **116**, 7127–7136 (2002). doi:10.1063/1.1464121

24. Luo, F., Cheng, Y., Chen, X.R., Cai, L.C., & Jing, F.Q., The melting curves and entropy of iron under high pressure. *J Chem Eng Data*, **56**, 2063–2070 (2011). doi:10.1021/je1010483
25. Shearer, P. & Masters, G., The density and shear velocity contrast at the inner core boundary. *Geophys J Int*, **102**, 491–408 (1990). doi:10.1111/j.1365-246X.1990.tb04481.x
26. Kubaschewski, O., *Iron-Binary Phase Diagrams* (New York: Springer-Verlag, 1982).
27. Morard, G., Andrault, D., Antonangeli, D., & Bouchet, J., Properties of iron alloys under the Earth's core conditions. *C R Geosci*, **346**, 130–139 (2014). doi:10.1016/j.crte.2014.04.007
28. Morard, G. et al., *In situ* determination of Fe–Fe3S phase diagram and liquid structural properties up to 65 GPa. *Earth Planet Sci Lett*, **272**, 620–626 (2008). doi:10.1016/j.epsl.2008.05.028
29. Mori, Y. et al., Melting experiments on Fe–Fe_3S system to 254 GPa. *Earth Planet Sci Lett*, **464**, 135–141 (2017). doi:10.1016/j.epsl.2017.02.021
30. Ozawa, H., Hirose, K., Yonemitsu, K., & Ohishi, Y., High-pressure melting experiments on Fe–Si alloys and implications for silicon as a light element in the core. *Earth Planet Sci Lett*, **456**, 47–54 (2016). doi:10.1016/j.epsl.2016.08.042
31. Kamada, S. et al., Phase relationships of the Fe–FeS system in conditions up to the Earth's outer core. *Earth Planet Sci Lett*, **294**, 94–100 (2010). doi:10.1016/j.epsl.2010.03.011
32. Li, J., Fei, Y., Mao, H.K., Hirose, K., & Shieh, S.R., Sulfur in the Earth's inner core. *Earth Planet Sci Lett*, **193**, 509–514 (2001). doi:10.1016/S0012-821X(01)00521-0
33. Kuwayama, Y. & Hirose, K., Phase relations in the system Fe–FeSi at 21 GPa. *Am Mineral*, **89**, 273–276 (2004). doi:10.2138/am-2004-2-303
34. Fischer, R.A. et al., Phase relations in the Fe–FeSi system at high pressures and temperatures. *Earth Planet Sci Lett*, **373**, 54–64 (2013). doi:10.1016/j.epsl.2013.04.035
35. Belonoshko, A.B., Rosengren, A., Burakovsky, L., Preston, D.L., & Johansson, B., Melting of Fe and Fe0.9375Si0.0625 at Earth's core pressures studied using *ab initio* molecular dynamics. *Phys Rev B*, **79**, 220102 (2009). doi:10.1103/PhysRevB.79.220102
36. Lin, J.-F. et al., Iron–nickel alloy in the Earth's core. *Geophys Res Lett*, **29**, 109–111 (2002). doi:10.1029/2002GL015089
37. Morard, G., Siebert, J., & Badro, J., Partitioning of Si and platinum group elements between liquid and solid Fe–Si alloys. *Geochim Cosmochim Acta*, **132**, 94–100 (2014). doi:10.1016/j.gca.2014.01.044
38. Anzellini, S., Dewaele, A., Mezouar, M., Loubeyre, P., & Morard, G., Melting of iron at Earth's inner core boundary based on fast X-ray diffraction. *Science*, **340**, 464–466 (2013). doi:10.1126/science.1233514
39. Dewaele, A. et al., Quasihydrostatic equation of state of iron above 2 Mbar. *Phys Rev Lett*, **97**, 29–32 (2006). doi:10.1103/PhysRevLett.97.215504
40. Mao, H.K., Wu, Y., Chen, L.C., & Shu, J.F., Static compression of iron to 300 GPa and Fe0.8Ni0.2 alloy to 260 GPa: implications for composition of the core. *J Geophys Res*, **95**, 21737–21742 (1990). doi:10.1029/JB095iB13p21737
41. Nakajima, Y. et al., Thermoelastic property and high-pressure stability of Fe7C3: implication for iron-carbide in the Earth's core. *Am Mineral*, **96**, 1158–1165 (2011). doi:10.2138/am.2011.3703

42. Seagle, C.T., Campbell, A.J., Heinz, D.L., Shen, G., & Prakapenka, V., Thermal equation of state of Fe3S and implications for sulfur in Earth's core. *J Geophys Res*, **111**, B06209 (2006). doi:10.1029/2005JB004091
43. Anderson, O.L. & Isaak, D.G., Another look at the core density deficit of Earth's outer core. *Phys Earth Planet Int*, **131**, 19–27 (2002). doi:10.1016/S0031-9201(02)00017-1
44. Anderson, W.W. & Ahrens, T.J., An equation of state for liquid iron and implications for the Earth's core. *J Geophys Res*, **99**, 4273–4284 (1994). doi:10.1029/93JB03158
45. Komabayashi, T. & Fei, Y., Internally consistent thermodynamic database for iron to the Earth's core conditions. *J Geophys Res*, **115**, B03202 (2010). doi:10.1029/2009JB006442
46. Bazhanova, Z.G., Oganov, A.R., & Gianola, O., Fe–C and Fe–H systems at pressures of the Earth's inner core. *Physics-Uspekhi*, **55**, 489–497 (2012). doi:10.3367/UFNe.0182.201205c .0521
47. Weerasinghe, G.L., Needs, R.J., & Pickard, C.J., Computational searches for iron carbide in the Earth's inner core. *Phys Rev B*, **84**, 1–7 (2011). doi:10.1103/PhysRev B.84.174110
48. Walker, D., Dasgupta, R., Li, J., & Buono, A., Nonstoichiometry and growth of some Fe carbides. *Contrib Mineral Petr*, **166**, 935–957 (2013). doi:10.1007/s00410-013-0900-7
49. Ono, S. & Mibe, K., Magnetic transition of iron carbide at high pressures. *Phys Earth Planet Int*, **180**, 1–6 (2010). doi:10.1016/j.pepi.2010.03.008
50. Sata, N. et al., Compression of FeSi, Fe3C, Fe0.95O, and FeS under the core pressures and implication for light element in the Earth's core. *J Geophys Res*, **115**, 1–13 (2010). doi:10.1029/2009JB006975
51. Rouquette, J. et al., Iron–carbon interactions at high temperatures and pressures. *Appl Phys Lett*, **12**, 121912 (2008). doi:10.1063/1.2892400
52. Liu, J., Lin, J.-F., Prakapenka, V., Prescher, C., & Yoshino, T., Phase relations of Fe–C and Fe7C3 up to 185 GPa and 5200 K: implication for the stability of iron carbide in the Earth's core. *Geophys Res Lett*, **43**, 12415–12422 (2016). doi:10.1002/2016GL071353
53. Walker, D., Li, J., Kalkan, B., & Clark, S.M., Thermal, compositional, and compressional demagnetization of cementite. *Am Mineral*, **100**, 2610–2624 (2015). doi:10.2138/am-2015-5306
54. Chen, B. et al., Experimental constraints on the sound velocities of cementite Fe3C to core pressures. *Earth Planet Sci Lett*, **494**, 164–171 (2018). doi:10.1016/j.epsl.2018.05.002
55. Gao, L. et al., Pressure-induced magnetic transition and sound velocities of Fe3C: implications for carbon in the Earth's inner core. *Geophys Res Lett*, **35**, L17306 (2008). doi:17310.11029/12008GL034817
56. Lin, J.F. et al., Magnetic transition in compressed Fe3C from X-ray emission spectroscopy. *Earth Planet Sci Lett*, **70**, 1–4 (2004). doi:10.1103/PhysRevB.70.212405
57. Mookherjee, M., Elasticity and anisotropy of Fe3C at high pressures. *Am Mineral*, **96**, 1530–1536 (2011). doi:10.2138/am.2011.3917
58. Prescher, C. et al., High Poisson's ratio of Earth's inner core explained by carbon alloying. *Nat Geosci*, **8**, 220–223 (2015). doi:10.1038/ngeo2370
59. Roberts, P.H., Jones, C.A., & Calderwood, A., Energy fluxes and Ohmic dissipation in the Earth's core, in *Earth's Core and Lower Mantle*, eds. C.A. Jones et al. (Abingdon: Taylor & Francis, 2003), pp. 100–129.

60. Vočadlo, L. et al., The effect of ferromagnetism on the equation of state of Fe3C studied by first-principles calculations. *Earth Planet Sci Lett*, **203**, 567–575 (2002). doi:10.1016/S0012-821X(02)00839-7
61. Li, J. et al., Compression of Fe3C to 30 GPa at room temperature. *Phys Chem Mineral*, **29**, 166–169 (2002). doi:10.1007/s00269-001-0224-4
62. Prescher, C. et al., Structurally hidden magnetic transitions in Fe3C at high pressures. *Phys Rev*, **85**, 6–9 (2012). doi:10.1103/PhysRevB.85.140402
63. Litasov, K.D. et al., Thermal equation of state and thermodynamic properties of iron carbide Fe_3C to 31 GPa and 1473 K. *J Geophys Res*, **118**, 1–11 (2013). doi:10.1002/2013JB010270
64. Chen, B. et al., Magneto-elastic coupling in compressed Fe7C3 supports carbon in Earth's inner core. *Geophys Res Lett*, **39**, 2–5 (2012). doi:10.1029/2012GL052875
65. Nakajima, Y. et al., Carbon-depleted outer core revealed by sound velocity measurements of liquid iron–carbon alloy. *Nature Comm*, **6**, 8942 (2015). doi:10.1038/ncomms9942
66. Morard, G. et al., Structure and density of Fe–C liquid alloys under high pressure. *J Geophys Res*, **122**, 7813–7823 (2017). doi:10.1002/2017JB014779
67. Das, T., Chatterjee, S., Ghosh, S., & Saha-Dasgupta, T., First-principles prediction of Si-doped Fe carbide as one of the possible constituents of Earth's inner core. *Geophys Res Lett*, **44**, 8776–8784 (2017). doi:10.1002/2017GL073545
68. Raza, Z., Shulumba, N., Caffrey, N.M., Dubrovinsky, L., & Abrikosov, I.A., First-principles calculations of properties of orthorhombic iron carbide Fe7C3 at the Earth's core conditions. *Phys Rev B*, **91**, 1–7 (2015). doi:10.1103/PhysRevB.91.214112
69. Chen, B. et al., Hidden carbon in Earth's inner core revealed by shear softening in dense Fe7C3. *Proc Natl Acad Sci USA*, **111**, 17755–17758 (2014). doi:10.1073/pnas.1411154111
70. Liu, J., Li, J., & Ikuta, D., Elastic softening in Fe7C3 with implications for Earth's deep carbon reservoirs. *J Geophys Res*, **121**, 1514–1524 (2016). doi:10.1002/2015JB012701
71. Mookherjee, M. et al., High-pressure behavior of iron carbide Fe7C3 at inner core conditions. *J Geophys Res B*, **116**, 1–13 (2011). doi:10.1029/2010JB007819
72. Caracas, R., The influence of carbon on the seismic properties of solid iron. *Geophys Res Lett*, **44**, 128–134 (2017). doi:10.1002/2015GL063478
73. Jimbo, I. & Cramb, A.W., The density of liquid iron–carbon alloys. *Metall Trans B*, **24**, 5–10 (1993). doi:10.1007/BF02657866
74. Badro, J., Cote, A.S., & Brodholt, J.P., A seismologically consistent compositional model of Earth's core. *Proc Natl Acad Sci USA*, **111**, 7542–7545 (2014). doi:10.1073/pnas.1316708111
75. Morard, G. et al., The Earth's core composition from high pressure density measurements of liquid iron alloys. *Earth Planet Sci Lett*, **373**, 169–178 (2013). doi:10.1016/j.epsl.2013.04.040
76. Brown, J.M. & McQueen, G., Phase transitions, Grüneisen parameter, and elasticity. *J Geophys Res*, **91**, 7485–7494 (1986). doi:10.1029/JB091iB07p07485
77. Lin, J.-F. et al., Sound velocities of hot dense iron: Birch's law revisited. *Science*, **308**, 1892–1894 (2005). doi:10.1126/science.1111724
78. Ohtani, E. et al., Sound velocity of hexagonal close-packed iron up to core pressures. *Geophys Res Lett*, **40**, 5089–5094 (2013). doi:10.1002/grl.50992
79. Singh, S.C., Taylor, M.A.J., & Montagner, J.P., On the presence of liquid in Earth's inner core. *Science*, **287**, 2471–2474 (2000). doi:10.1126/science.287.5462.2471

80. Li, Y., Vočadlo, L., Brodholt, J., & Wood, I.G., Thermoelasticity of Fe7C3 under inner core conditions. *J Geophys Res*, **B121**, 5828–5837 (2016). doi:10.1002/2016JB013155
81. Martorell, B., Brodholt, J., Wood, I.G., & Vočadlo, L., The effect of nickel on the properties of iron at the conditions of Earth's inner core: *ab initio* calculations of seismic wave velocities of Fe–Ni alloys. *Science*, **365**, 143–151 (2013). doi:10.1016/j.epsl.2013.01.007
82. Ichikawa, H., Tschuchiya, T., & Tange, Y., The P–V–T equation of state and thermodynamic properties of liquid iron. *J Geophys Res*, **119**, 240–252 (2014). doi:10.1002/2013JB010732.Received
83. Vočadlo, L., Alfè, D., Gillan, M.J., & Price, G.D., The properties of iron under core conditions from first principles calculations. *Phys Earth Planet Int*, **140**, 101–125 (2003). doi:10.1016/j.pepi.2003.08.001
84. Kantor, A.P. et al., Sound wave velocities of fcc Fe–Ni alloy at high pressure and temperature by mean of inelastic X-ray scattering. *Phys Earth Planet Int*, **164**, 83–89 (2007). doi:10.1016/j.pepi.2007.06.006
85. Souriau, A. & Poupinet, G., The velocity profile at the base of the liquid core from PKP(BC+Cdiff) data: an argument in favor of radial inhomogeneity. *Geophys Res Lett*, **18**, 2023–2026 (1991). doi:10.1029/91GL02417
86. Wookey, J. & Helffrich, G., Inner-core shear-wave anisotropy and texture from an observation of PKJKP waves. *Nature*, **454**, 873–876 (2008). doi:10.1038/nature07131
87. Mao, H.K. et al., Elasticity and rheology of iron above 220 GPa and the nature of the Earth's inner core. *Nature*, **396**, 741–743 (1998). doi:10.1038/25506
88. Antonangeli, D. et al., Elastic anisotropy in textured hcp-iron to 112 GPa from sound wave propagation measurements. *Earth Planet Sci Lett*, **225**, 243–251 (2004). doi:10.1016/j.epsl.2004.06.004
89. Mao, H.K. et al., Phonon density of states of iron up to 153 gigapascals. *Science*, **292**, 914–916 (2001). doi:10.1126/science.1057670
90. Murphy, C.A., Jackson, J.M., & Sturhahn, W., Experimental constraints on the thermodynamics and sound velocities of hcp-Fe to core pressures. *J Geophys Res*, **118**, 1999–2016 (2013). doi:10.1002/jgrb.50166
91. Lin, J.-F. et al., Sound velocities of iron–nickel and iron–silicon alloys at high pressures. *Geophys Res Lett*, **30**, 1–4 (2003). doi:10.1029/2003GL018405
92. Gao, L. et al., Sound velocities of compressed Fe3C from simultaneous synchrotron X-ray diffraction and nuclear resonant scattering measurements. *J Synchrotron Rad*, **16**, 714–722 (2009). doi:10.1107/S0909049509033731
93. Nikolussi, M. et al., Extreme elastic anisotropy of cementite, Fe3C: first-principles calculations and experimental evidence. *Scripta Mater*, **59**, 814–817 (2008). doi:10.1016/j.scriptamat.2008.06.015
94. Gao, L. et al., Effect of temperature on sound velocities of compressed Fe3C, a candidate component of the Earth's inner core. *Earth Planet Sci Lett*, **309**, 213–220 (2011). doi:10.1016/j.epsl.2011.06.037
95. Huang, H. et al., Shock compression of Fe–FeS mixture up to 204 GPa. *Geophys Res Lett*, **40**, 687–691 (2013). doi:10.1002/grl.50180
96. Jing, Z. et al., Sound velocity of Fe–S liquids at high pressure: implications for the Moon's molten outer core. *Earth Planet Sci Lett*, **396**, 78–87 (2014). doi:10.1016/j.epsl.2014.04.015

97. Umemoto, K. et al., Liquid iron sulfur alloys at outer core conditions by first-principles calculations. *Geophys Res Lett*, **41**, 6712–6717 (2014). doi:10.1002/2014GL061233
98. Kawaguchi, S.I. et al., Sound velocity of liquid Fe–Ni–S at high pressure. *J Geophys Res*, **122**, 3624–3634 (2017). doi:10.1002/2016JB013609
99. Huang, H. et al., Evidence for an oxygen-depleted liquid outer core of the Earth. *Nature*, **479**, 513–516 (2011). doi:10.1038/nature10621
100. Caracas, R., The influence of hydrogen on the seismic properties of solid iron. *Geophys Res Lett*, **42**, 3780–3785 (2015). doi:10.1002/2015GL063478
101. Umemoto, K. & Hirose, K., Liquid iron–hydrogen alloys at outer core conditions by first-principles calculations. *Geophys Res Lett*, **42**, 7513–7520 (2015). doi:10.1002/2015GL 065899
102. Lin, J.F. et al., Magnetic transition and sound velocities of Fe3S at high pressure: implications for Earth and planetary cores. *Phy Rev B*, **226**, 33–40 (2004). doi:10.1016/j.epsl.2004.07.018
103. Badro, J. et al., Effect of light elements on the sound velocities in solid iron: implications for the composition of Earth's core. *Earth Planet Sci Lett*, **254**, 233–238 (2007). doi:10.1016/j.epsl.2006.11.025
104. Mao, W.L. et al., Nuclear resonant X-ray scattering of iron hydride at high pressure. *Geophys Res Lett*, **31**, L15618 (2004). doi:10.11029/2004GL020541
105. Shibazaki, Y. et al., Effect of hydrogen on the melting temperature of FeS at high pressure: implications for the core of Ganymede. *Earth Planet Sci Lett*, **301**, 153–158 (2013). doi:10.1016/j.epsl.2010.10.033
106. Huang, H. et al., Melting behavior of Fe–O–S at high pressure: a discussion on the melting depression induced by O and S. *J Geophys Res*, **115** (2010). doi:10.1029/2009JB006514
107. Antonangeli, D. et al., Composition of the Earth's inner core from high-pressure sound velocity measurements in Fe–Ni–Si alloys. *Earth Planet Sci Lett*, **295**, 292–296 (2010). doi:10.1016/j.epsl.2010.04.018
108. McNamara, A.K., Garnero, E.J., & Rost, S., Tracking deep mantle reservoirs with ultra-low velocity zones. *Earth Planet Sci Lett*, **299**, 1–9 (2010). doi:10.1016/j.epsl.2010.07.042
109. Fiquet, G. et al., Melting of peridotite to 140 gigapascals. *Science*, **329**, 1516–1518 (2010). doi:10.1016/j.epsl.2010.04.018
110. Lord, O.T. et al., The FeSi phase diagram to 150 GPa. *J Geophys Res*, **115**, 1–9 (2010). doi:10.1029/2009JB006528
111. Liu, J., Li, J., Hrubiak, R., & Smith, J.S., Origin of ultra-low velocity zones through mantle-derived metallic melt. *Proc Natl Acad Sci ISA*, **113**, 5547–5551 (2016). doi:10.1073/pnas.1519540113
112. Andrault, D. et al., Melting of subducted basalt at the core-mantle boundary. *Science*, **344**, 892–895 (2014). doi:10.1126/science.1250466
113. Terasaki, H. et al., Liquidus and solidus temperatures of a Fe–O–S alloy up to the pressures of the outer core: implication for the thermal structure of the Earth's core. *Earth Planet Sci Lett*, **304**, 559–564 (2011). doi:10.1016/j.epsl.2011.02.041
114. Tsuno, K. & Ohtani, E., Eutectic temperatures and melting relations in the Fe–O–S system at high pressures and temperatures. *Phys Chem Mineral*, **36**, 9–17 (2009). doi:10.1007/s00269-008-0254-2
115. Lodders, K., Solar system abundances and condensation temperatures of the elements. *Astrophys J*, **591**, 1220–1247 (2003). doi:1210.1086/375492

116. Zhang, C.W. et al., Electrical resistivity of Fe–C alloy at high pressure: effects of carbon as a light element on the thermal conductivity of the Earth's core. *J Geophys Res*, **123**, 3564–3577 (2018). doi:10.1029/2017JB015260
117. Rudge, J.F., Kleine, T., & Bourdon, B., Broad bounds on Earth's accretion and core formation constrained by geochemical models. *Nature Comms*, **3**, 439–443 (2010). doi:10.1038/ngeo872
118. Albarède, F., Volatile accretion history of the terrestrial planets and dynamic implications. *Nature*, **461**, 1227–1233 (2009). doi:10.1038/nature08477
119. Hayden, L. & Watson, B., Grain boundary mobility of carbon in Earth's mantle: a possible carbon flux from the core. *Proc Natl Acad Sci USA*, **105**, 8537–8541 (2008). doi:10.1073 pnas.0710806105
120. Dorfman, S.M. et al., Carbonate stability in the reduced lower mantle. *Earth Planet Sci Lett*, **498**, 84–91 (2018). doi:10.1016/j.epsl.2018.02.035
121. Scott, H.P., Williams, Q., & Knittle, E., Stability and equation of state of Fe_3C to 73 GPa: implications for carbon in the Earth's core. *Geophys Res Lett*, **28**, 1875–1878 (2001). doi:10.1029/2000GL012606
122. Dodd, S.P., Saunders, G.A., Cankurtaran, M., James, B., & Acet, M., Ultrasonic study of the temperature and hydrostatic-pressure dependences of the elastic properties of polycrystalline cementite (Fe3C). *Phys Status Solidi A*, **198**, 272–281 (2003). doi:10.1002/pssa.200306613
123. Fiquet, G., Badro, J., Gregoryanz, E., Fei, Y., & Occelli, F., Sound velocity in iron carbide (Fe_3C) at high pressure: implications for the carbon content of the Earth's inner core. *Phys Earth Planet Inter*, **172**, 125–129 (2009). doi:10.1016/j.pepi.2008.05.016
124. Sanloup, C. et al., Density measurements of liquid Fe–S alloys at high-pressure. *Earth Planet Sci Lett*, **27**, 811–814 (2000). doi:10.1029/1999GL008431
125. Balog, P.S., Secco, R.A., Rubie, D.C., & Frost, D.J., Equation of state of liquid Fe-10 wt % S: implications for the metallic cores of planetary bodies. *J Geophys Res*. **108**, B2 (2003). doi:10.1029/2001jb001646
126. Nishida, K. et al., Towards a consensus on the pressure and composition dependence of sound velocity in the liquid Fe–S system. *Phys Earth Planet Int*, **257**, 230–239 (2016). doi:10.1016/j.pepi.2016.06.009
127. Shimoyama, Y. et al., Thermoelastic properties of liquid Fe–C revealed by sound velocity and density measurements at high pressure. *J Geophys Res*, **121**, 7984–7995 (2016). doi:10.1002/2016JB012968
128. Sanloup, C., van Westrenen, W., Dasgupta, R., Maynard-Casely, H., & Perrillat, J.P., Compressibility change in iron-rich melt and implications for core formation models. *Earth Planet Sci Lett*, **306**, 118–122 (2011). doi:10.1016/j.epsl.2011.03.039
129. Terasaki, H. et al., Density measurement of Fe3C liquid using X-ray absorption image up to 10 GPa and effect of light elements on compressibility of liquid iron. *J Geophys Res*, **115**, 1–7 (2010). doi:10.1029/2009JB006905
130. Yu, X. & Secco, R.A., Equation of state of liquid Fe–17 wt%Si to 12 GPa. *High Pressure Res*, **28**, 19–28 (2008). doi:10.1080/08957950701882138
131. Sanloup, C., Fiquet, G., Gregoryanz, E., Morard, G., & Mezouar, M., Effect of Si on liquid Fe compressibility: implications for sound velocity in core materials. *Geophys Res Lett*, **31**, 7 (2004). doi:10.1029/2004GL019526
132. Komabayashi, T., Thermodynamicsof melting relations in the system Fe–FeO at high pressure: implications for oxygen in the Earth's core. *J Geophys Res*, **119**, 4164–4177 (2014). doi:10.1002/2014JB010980